Journal of Power Sources 454 (2020) 227930

Contents lists available at ScienceDirect

Journal of Power Sources

journal homepage: www.elsevier.com/locate/jpowsour

Thermodynamically consistent reduced dimensionality electrochemical model for proton exchange membrane fuel cell performance modelling and control

Andraž Kravos [a], Daniel Ritzberger [b], Gregor Tavčar [a], Christoph Hametner [c], Stefan Jakubek [b], Tomaž Katrašnik [a,*]

[a] University of Ljubljana, Faculty of Mechanical Engineering, LICeM, Slovenia
[b] Institute of Mechanics and Mechatronics, TU Wien, Austria
[c] CD Laboratory for Innovative Control and Monitoring of Automotive Powertrain Systems, TU Wien, Austria

HIGHLIGHTS

- Advanced 0D thermodynamically consistent electrochemical model of PEMFC is derived.
- Identifiability of calibration parameters was proven by sensitivity analysis.
- Ease of parametrisation on the small calibration data is achieved.
- Model exhibit good extrapolation capabilities beyond calibrated operational area.
- Newly derived model is applicable in on-line monitoring and control applications.

ARTICLE INFO

Keywords:
PEM fuel cells
Electrochemical model
Performance modelling
Reduced dimensionality models
Parameter sensitivity
Observers

ABSTRACT

The reduction and prevention of degradation effects of proton exchange membrane fuel cells calls for precise on-line monitoring and control tools such as coupled virtual observers. To present significant progress in the area of computationally fast electrochemical models used in observer applications, this paper provides the derivation of a zero-dimensional thermodynamically consistent electrochemical model for proton exchange membrane fuel cells performance modelling and control. The model is further extended to accommodate the transport of gaseous species along the channel and through gas diffusion layer, yielding a quasi-one-dimensional electrochemical model. In addition, the presented work features the determination of an optimal set of calibration parameters proposed and based on mathematical and physical rationale, which is further supported with parameter sensitivity analysis. Multiple validation steps against polarisation curves at different operational points confirm the capability of the newly developed model to replicate experimental data. Furthermore, investigation in models generalisation capabilities shows that the model exhibits very good extrapolation capabilities for operation points outside the calibrated variation space of parameters. Additionally, the newly developed model can be successfully parametrised with little effort on a small calibration data set. These features position the proposed modelling framework as a beyond state-of-the-art model for virtual observers.

1. Introduction

Increasing health concerns regarding local air quality pave the way for more and more strict emission regulations across the energy and transport sectors. As an answer to this requirement, both electrification and hybridisation of powertrains are emerging as a feasible solution for the transport sector. Since plug-in hybrid vehicles offer a limited emission free range and since battery electric vehicles are characterized by a high ratio between charging times and available electrical driving range [1], the use of low temperature hydrogen fuelled proton exchange membrane fuel cells (LT-PEMFC) coupled with smaller battery packs in hydrogen-powered vehicles appears as a viable solution with zero tank-to-wheel emissions. They are characterized by short refuelling

* Corresponding author.
E-mail address: tomaz.katrasnik@fs.uni-lj.si (T. Katrašnik).
URL: http://lab.fs.uni-lj.si/LICeM/ (T. Katrašnik).

https://doi.org/10.1016/j.jpowsour.2020.227930
Received 17 October 2019; Received in revised form 3 February 2020; Accepted 17 February 2020
Available online 6 March 2020

Nomenclature

α	Charge transfer coefficient
Δ	Change, difference
δ	Width
η	Overpotential
λ	Stoichiometric ratio
D	Binary diffusion coefficients
ω	Kinetic reaction order
A	Energy needed to get to transition state on the cathode side
B	Energy needed to get to transition state on the anode side
C	Concentration
CD	Combined diffusive parameter
D	Ternary diffusion coefficients
E	Energy
e^-	Electron
e_0	Basic charge
F	Faraday constant
g	Specific Gibbs free energy
H^+	Proton
H_2	Hydrogen
H_2O	Water
I	Current
i	Current density
I_0	Intrinsic exchange current
k	Reaction rate
k_B	Boltzmann constant
O_2	Oxygen
R	Resistance
R_g	Gas constant
s	Specific entropy
T	Temperature
U	Potential
Z	Number of electrons transferred in the electrochemical reaction
a	Anode
AIC	Akaike Information Criterion
BV	Butler - Volmer
c	Cathode
FC	Fuel Cell
GDL	Gas Diffusion Layer
HiL	Hardware-in-the-Loop
LT	Low Temperature
OXA	Oxidation on the Anode
OXC	Oxidation on the Cathode
p	Products
PEM	Proton Exchange Membrane
r	Reactants
RDA	Reduction on the Anode
RDC	Reduction on the Cathode
ref	Reference
RMSD	Root Mean Square Deviation
s	Spectator species
SoF	State of Function
SoH	State of Health
SoOC	State of Operational Conditions
TC	Thermodynamically Consistent

times and long ranges [2,3], approaching those of conventional vehicles. Furthermore, hydrogen-powered vehicles are also compatible with the emerging sector of coupling of energy system solutions, where excess peaks in electricity production due to renewable sources, especially wind turbines and photovoltaic cells, can be utilized for hydrogen production via electrolysis and can afterwards be converted back to electricity in LT-PEMFCs [4].

LT-PEMFCs in general operate in transient conditions. A highly dynamic operation is in particular characteristic for vehicle applications. Even if a battery pack is used for accommodating high transients in power demand, it is to be kept as small as possible due to packaging, mass and cost constraints. A highly dynamic operation of LT-PEMFCs calls for precise on-line monitoring and control solutions, such as a framework of coupled virtual observers. The aim is a reduction and prevention of degradation effects and their influence on the remaining useful life, while retaining high performance of the FC.

Most comprehensive applications tackling the aforementioned problems usually rely on three coupled virtual observer models (Fig. 1), namely state of operational conditions (SoOC), state of health (SoH) and state of function (SoF). Traditionally, observers featuring data driven models or reduced dimensionality models (i.e. 0D, quasi-1D, etc.) e.g. Refs. [5–9] that are parametrised by experimental data, or by using other models with a sufficiently high prediction capability, generality and sufficiently short computational times to allow for the execution of large designs of experiments to determine an ideal operational strategy. Models used in these parametrisation procedures must foremost be computationally fast to enable the application of control strategies in real time. Besides computational speed it is of utmost importance that models used for observer parametrisation have good extrapolation capabilities, which enables their parametrisation on small data sets, and which have direct synergistic effects with the last important property of these models, which is that they are easy to parametrise.

Based on the aforementioned necessary properties of

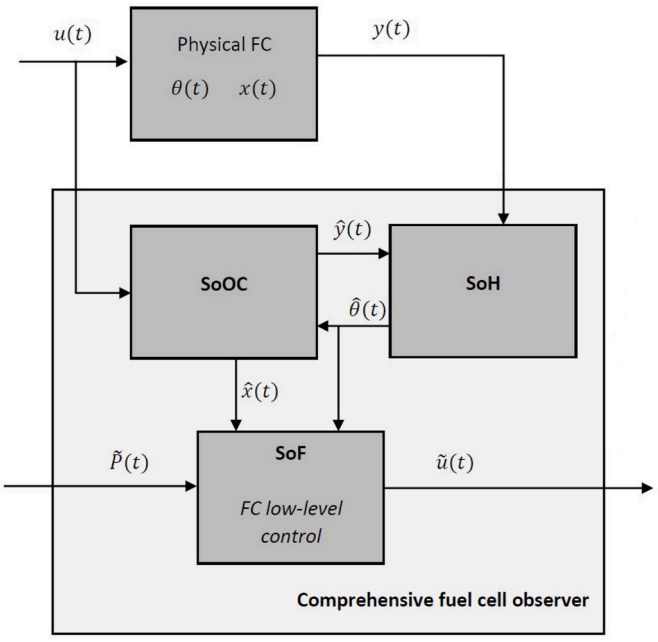

Fig. 1. Schematic representation of the comprehensive FC observer.

electrochemical models used for virtual observer parametrisation, data driven models, which are often applied in the system level analyses, have limited applicability in studies aimed at combined performance and service life optimisations. This is reasoned by the fact that the accuracy of data driven models generally, does not reach beyond the

trained variation space of parameters and due to the fact that training data driven models on a variation space with a very large dimensionality proves to be cumbersome due to the effects of i.e. the curse of dimensionality [10]. This reasoning is fully applicable in the area of a FC, where performance modelling alone, presented in Refs. [11–17], possesses a problem with multiple degrees of freedom (pressure, temperature, stoichiometry, concentrations, etc.).

This motivated the use of the comprehensive observers (Fig. 1), which are usually built around computationally fast reduced dimensionality electrochemical models featuring a more profound mechanistic basis. These models are also parametrised based on the higher fidelity PEMFC models or experimental data. They feature better prediction capability outside the trained variation space, as they use a more consistent thermodynamic basis. To achieve a high prediction capability of the model in the entire current range net reaction rates are commonly modelled by the Butler-Volmer (BV) equation:

$$j = j_0 \left(e^{\frac{\alpha e_0 Z U}{k_B T}} - e^{\frac{(1-\alpha) e_0 Z U}{k_B T}} \right). \tag{1}$$

However, devising a reduced dimensionality performance model revolving around the BV proves to be cumbersome, due to problems with finding its inverse function with respect to voltage. This is utmost importance to increase ease of parametrisation, which is fairly easy when applied to simplified expression for overall voltage drop of the FC: $\Delta U = \Delta U_{act} + \Delta U_{ohm} + \Delta U_{conc}$. Consequentially, different approximations that were made in literature, found reduced dimensionality models to successfully tackle this problem.

Therefore, reduced dimensionality electrochemical FC models that possess all of three needed properties for successfully virtual observer parametrisation can in general be categorised as:

1. Electrochemical models based on the Tafel equation:

$$j = j_0 e^{\frac{\alpha e_0 Z U}{k_B T}}, \tag{2}$$

which is derived from the BV equation with the approximation that the forward-reaction direction overshadows reactions in the backward direction. This is a reasonable approximation for operational points with high current densities and consequential high activation overvoltages. However, it possesses a significant downside in the low current density region, where the approximation error increases exponentially when current density approaches zero, which inevitably means that the activation losses cannot be well defined. This approach can be found in publications [18–28].

2. Electrochemical models based on the Tafel equation - Equation (2) extended by different corrections for the low current density region with the aim of reducing calibration error of the terms in the expression for activation losses. In Refs. [29,30] the linearisation of the Tafel equation - Equation (2) for the anode side:

$$j = j_{0_a} \frac{\alpha e_0 Z_a U_a}{k_B T}, \tag{3}$$

and application of the Tafel equation - Equation (2) for the cathode side is proposed to address this problem. On the other hand, in Refs. [31–33] a posteriori substitution of natural logarithm in Tafel equation with sinus hyperbolicus is performed (Equations (A.1),(A.3) and (A.5)). Proposed substitution successfully reduces the overall error in the low current density region, however it leads to incorrectly positioned individual terms in the equation for activation losses (Equation (A.5)), which can influence both the calibration procedure and model performance.

To comply with the above listed objectives and present progress in the area of computationally efficient electrochemical FC models, this paper outlines the derivation of a novel 0D thermodynamically consistent (TC) FC electrochemical model presented in Section 2. In addition, it is consistently extended to accommodate the diffusive transport of gaseous species in the gas diffusion layer (GDL) and along the channels, thus resulting in a quasi-1D TC FC electrochemical model. Thermodynamically consistent derivation of the model also ensures a consistent analytically derived expression for the polarisation curve in low current density regions, where parameters describing activation losses are usually prone to calibration error. This is a very important merit of the proposed model, since errors in activation losses influence the whole polarisation curve, and thus the prediction of PEMFC performance. To successfully reduce calibration times of the TC FC electrochemical model on small data sets, which is crucial for enhanced applicability of the model, a determination of the optimal set of calibration parameters is performed in Section 3. In Section 4 the newly developed TC FC electrochemical model is benchmarked against state-of-the-art reduced dimensionality electrochemical models with the aim of assessing its robustness and extrapolation capabilities on polarisation curves at different operational conditions. Furthermore, the effects of an optimal set of calibration parameters on convergence speed during the calibration procedure are assessed. In Section 5 the main conclusions are summarized.

2. Devising of 0D electrochemical models

This section presents all the necessary derivation steps to obtaining the TC FC electrochemical model and the key approximations introduced during the derivation of models proposed in Refs. [21–27,29,31–33]. To structure this procedure, the derivation is divided into four separate subsections, namely:

Derivation of basic governing equations in a thermodynamically consistent manner and its formulation in a compact form that is used for the derivation of simplified versions.

Simplifications of the BV equation in published models, where these simplifications have consequential effects on performance, generality and prediction capability of the models.

Consistent treatment of forward and backward reactions in BV equation, which consequentially results in the derivation of the 0D TC FC electrochemical model.

Simplified 1D transport of gaseous species in the GDL, where the aforementioned 0D TC electrochemical model is extended with a simplified 1D approach to accommodate the diffusive transport of species in the GDL.

Simplified 1D transport of gaseous species along the channel, where effects of finite stoichiometric ratio are taken into account by analytical solution of convection-diffusion equation.

The derivation of the steady state TC electrochemical model is based on the following assumptions:

I The problem is isothermal, however the electrodes could have different temperatures.
II Charge transfer coefficient in electrochemical reactions is assumed to take the value of 0.5.
III Concentration of electrons and protons are approximately uniform in the electrodes.

IV Catalyst layers are infinitely thin and a uniform potential is assumed for them.
V The gasses are treated as ideal.
VI The diffusion constants are pressure insensitive.
VII The diffusion system is always bicomponential and therefore described by scalar diffusion constant.
VIII There is no liquid water in the GDLs and channels.
IX There is no convective transport in the GDLs.
X The membrane assumes no gas crossover.
XI The membrane is ideally and constantly hydrated at all times.

Assumption IV is valid for newer, thinner catalyst layers with reduced size of aggregates and agglomerates of catalyst/support. For effects of variation of the oxygen concentration and overpotential through the catalyst layer depth readers are referred to book [33]. The rest of assumptions are all within the sets of common assumptions made by other 0D and 1D reduced dimensionality models presented in Refs. [18–33]. However it should be pointed out that liquid water dynamics highly influence the PEM FC performance. Therefore, modelling assumption of no liquid water in the system can be made only, due to the fact that experiments were performed under constant stoichiometry and constant temperature for individual polarisation curves and that polarisation curves were logged after steady state operation has been reached. Presence of liquid water is in this cases reflected through the combined diffusivity parameter, therefore, liquid water fraction is already taken into account when combined diffusivity parameter is being calibrated.

2.1. Basic governing equations

The FC voltage can at any given time be approximated with a summation of five individual terms [34], namely open circuit voltage on the cathode - U_c^{OC} and anode side - U_a^{OC} (sometimes written as a single term), voltage drop due to ohmic resistance - RI, reaction kinetics overvoltage on the cathode - η_c and anode side η_a:

$$U = U_c^{OC} + \eta_c - RI - U_a^{OC} - \eta_a. \tag{4}$$

The derivation of individual terms starts with expression for the kinetics of anode and cathode reactions, which can be written as [35]:

$$j_{RDC} = \left(\frac{C(e^-)}{C_{ref}(e^-)}\right)^{\omega_{e^-}} \left(\frac{C(H^+)}{C_{ref}(H^+)}\right)^{\omega_{H^+}} \left(\frac{C(O_2)}{C_{ref}(O_2)}\right)^{\omega_{O_2}} \cdot k_{RDC} \cdot \mathrm{e}^{-\frac{A}{k_B T}}, \tag{5}$$

$$j_{OXC} = \left(\frac{C(H_2O)}{C_{ref}(H_2O)}\right)^{\omega_{H_2O}} k_{OXC} \cdot \mathrm{e}^{\left(-\frac{A+\Delta g_c - U_c e_0 Z_c}{k_B T}\right)}, \tag{6}$$

$$j_{RDA} = \left(\frac{C(e^-)}{C_{ref}(e^-)}\right)^{\omega_{e^-}} \left(\frac{C(H^+)}{C_{ref}(H^+)}\right)^{\omega_{H^+}} k_{RDA} \cdot \mathrm{e}^{-\frac{B+\Delta g_a - U_a e_0 Z_a}{k_B T}}, \tag{7}$$

$$j_{OXA} = \left(\frac{C(H_2)}{C_{ref}(H_2)}\right)^{\omega_{H_2}} k_{OXA} \cdot \mathrm{e}^{\left(-\frac{B}{k_B T}\right)}, \tag{8}$$

where $j_{RDC}, j_{OXC}, j_{RDA}$ and j_{OXA} are the reaction rate of cathode reduction, cathode oxidation, anode reduction and anode oxidation, respectively. $k_{RDC}, k_{OXC}, k_{RDA}$ and k_{OXA} are reaction rate constants, k_B is the Boltzmann constant, T is the temperature, e_0 is the elementary charge, Δg_a and Δg_c are the difference in specific Gibbs free energy between reactants and products on the anode and cathode side, Z_a and Z_c are the number of electrons transferred in the electrochemical reaction on the anode and cathode side, values of ω_{e^-}, ω_{H^+}, ω_{O_2}, ω_{H_2O} and ω_{H_2} represent kinetic reaction orders of the respective species participating in the reaction. $C(e^-)$, $C(H^+)$, $C(O_2)$, $C(H_2O)$, $C(H_2)$ are concentrations of electrons, protons, oxygen, water and hydrogen, respectively. On the other hand, their reference concentrations are given as: $C_{ref}(e^-)$, $C_{ref}(H^+)$, $C_{ref}(O_2)$, $C_{ref}(H_2O)$, $C_{ref}(H_2)$. Whereas, $A = A(U)$ and $B = B(U)$ represent energy needed to get to the transition state:

$$A(U) = A_0 + \alpha_c U_c e_0 Z_c, \tag{9}$$

$$B(U) = B_0 + \alpha_a U_a e_0 Z_a, \tag{10}$$

where α_a and α_c are the charge transfer coefficients on the anode and cathode side, $A_0 = A(U=0)$ and $B_0 = B(U=0)$ represent energy needed to get to transition state at $U = 0$ on the cathode and anode sides, respectively.

From this point onward it is assumed that the terms $(\tilde{C}_{e^-})^{\omega_{e^-}}$ and $(\tilde{C}_{H^+})^{\omega_{H^+}}$, representing concentration of electrons and protons are approximately uniform in the electrodes. Therefore, they can be merged with k_{RDC} and k_{RDA} to form k^*_{RDC} and k^*_{RDA}, respectively. For the sake of brevity of this paper from this point onward only derivation procedure for cathode side will be shown, since derivation for anode side is analogous. Cathodic net reaction rate (j_c) is [35]:

$$j_c = j_{RDC} - j_{OXC}, \tag{11}$$

Inserting Equations (5) and (6), which express the kinetics of cathode reactions into Equation (11), and replacing $\frac{C(H_2O)}{C_{ref}(H_2O)}$ with $\tilde{C}_{H_2O}$, $\frac{C(O_2)}{C_{ref}(O_2)}$ with $\tilde{C}_{O_2}$, the following expression for net reaction rates is obtained:

$$j_c = (\tilde{C}_{O_2})^{\omega_{O_2}} k^*_{RDC} \cdot \mathrm{e}^{-\frac{A}{k_B T}} - (\tilde{C}_{H_2O})^{\omega_{H_2O}} k_{OXC} \cdot \mathrm{e}^{\left(-\frac{A+\Delta g_c - U_c e_0 Z_c}{k_B T}\right)}. \tag{12}$$

Net reaction rates given in Equation (12) are functions of potentials on the cathode side of the FC, which can be written as summation of over-voltage and open circuit voltage:

$$U_c = U_c^{OC} + \eta_c. \tag{13}$$

With the obtained expressions featuring open circuit voltage Equation (12) combined with (13) can be rewritten as:

$$j_c = \left(\tilde{C}_{O_2}\right)^{\omega_{O_2}} k^*_{RDC} \cdot \mathrm{e}^{-\frac{A}{k_B T}} - \left(\tilde{C}_{H_2O}\right)^{\omega_{H_2O}} k_{OXC} \cdot \mathrm{e}^{\left(-\frac{A+\Delta g_c - \left(U_c^{OC}+\eta_c\right) e_0 Z_c}{k_B T}\right)}. \tag{14}$$

In the case of FC disconnection from the circuit, the open circuit voltage is obtained, which means that the over-potentials are 0 and also the current is 0 ($U_c^{OC} \rightarrow j_c = 0, \quad \eta_c = 0$). Using this information in Equation (14), the open circuit voltage can be obtained. Firstly, expression $U_c^{OC} \rightarrow j_c = 0, \quad \eta_c = 0$ is used on Equation (14) and the result is then rearranged in a way that gives the Nernst equation for the open circuit voltage, where net reaction rates of reduction and oxidation on the cathode side are in equilibrium. Therefore, the expression for open circuit voltage on the cathode side can be written as:

$$U_c^{OC} = \frac{k_B T}{e_0 Z_c} \ln\left((\tilde{C}_{H_2O})^{-\omega_{H_2O}} \cdot (\tilde{C}_{O_2})^{\omega_{O_2}}\right) + \frac{k_B T}{e_0 Z_c} \ln\left(\frac{k^*_{RDC}}{k_{OXC}}\right) + \frac{\Delta g_c^0}{e_0 Z_c} + \frac{(T - T_{ref})\Delta s_c}{e_0 Z_c}. \tag{15}$$

Inserting the expression of U_c^{OC} as defined in Equation (15) into Equation (14) gives us the following:

$$j_c = \left(e^{-\frac{A_0}{k_B T}} (\tilde{C}_{O_2})^{\omega_{O_2}} k^*_{RDC} ((\tilde{C}_{O_2})^{\omega_{O_2}} (\tilde{C}_{H_2O})^{-\omega_{H_2O}})^{-\alpha_c} \left(\frac{k^*_{RDC}}{k_{OXC}}\right)^{-\alpha_c} \cdot e^{-\frac{\alpha_c \Delta g_c}{k_B T}} e^{-\frac{\alpha_c e_0 Z_c \eta_c}{k_B T}} - (\tilde{C}_{H_2O})^{\omega_{H_2O}} k_{OXC} ((\tilde{C}_{O_2})^{\omega_{O_2}} (\tilde{C}_{H_2O})^{-\omega_{H_2O}})^{1-\alpha_c} \cdot \left(\frac{k^*_{RDC}}{k_{OXC}}\right)^{1-\alpha_c} e^{\frac{(1-\alpha_c)\Delta g_c}{k_B T}} e^{\frac{(1-\alpha_c) e_0 Z_c \eta_c}{k_B T}} e^{-\frac{\Delta g_c}{k_B T}} \right), \quad (16)$$

Based on chemical kinetic reaction orders $\omega_{O_2} = 1$ and $\omega_{H_2O} = 2$ can be determined. With that and taking into account that for specific Gibbs free energy it can be written: $\Delta g = \Delta g^0 + \Delta s(T - T^0)$, the expression known as the BV equation with all thermodynamically based parameters is obtained for the cathode side:

$$j_c = e^{-\frac{A_0}{k_B T}} e^{-\frac{\alpha_c \Delta s^0_c}{k_B T}} e^{-\frac{\alpha_c \Delta s_c (T - T^0)}{k_B T}} e^{-\alpha_c \cdot \ln\left(\frac{k^*_{RDC}}{k_{OXC}}\right)} (\tilde{C}_{O_2})^{(1-\alpha_c)} \cdot (\tilde{C}_{H_2O})^{2\alpha_c} k^*_{RDC} \left(\underbrace{e^{-\frac{\alpha_c e_0 Z_c \eta_c}{k_B T}}}_{(A)} - \underbrace{e^{\frac{(1-\alpha_c) e_0 Z_c \eta_c}{k_B T}}}_{(B)} \right), \quad (17)$$

and equivalently for the anode side:

$$j_a = e^{-\frac{B_0}{k_B T}} e^{-\frac{\alpha_a \Delta s^0_a}{k_B T}} e^{-\frac{\alpha_a \Delta s_a (T - T^0)}{k_B T}} e^{-\alpha_a \cdot \ln\left(\frac{k_{OXA}}{k^*_{RDA}}\right)} (\tilde{C}_{H_2})^{(2\alpha_a)} \cdot k^*_{RDA} \left(\underbrace{e^{\frac{\alpha_a e_0 Z_a \eta_a}{k_B T}}}_{(A)} - \underbrace{e^{-\frac{(1-\alpha_a) e_0 Z_a \eta_a}{k_B T}}}_{(B)} \right) \quad (18)$$

2.2. Simplifications of BV equation in published models

The majority of published works use the Tafel equation instead of the whole BV equation to describe how the net reaction rates depend on overpotential, thus they fall in the first category of reduced dimensionality electrochemical models as presented in the Introduction. The Tafel equation is obtained from the BV equation when the forward-reaction direction (Term (A) in Equations (17) and (18)) is taken as dominant over reactions in the backward-reaction direction (Term (B) in Equations (17) and (18)), which are therefore neglected. Expressions obtained with Tafel approximation are with the purpose of comparison with TC electrochemical model presented in detail in (Appendix A) Equations (A.1), (A.2), (A.3) and (A.4). It has to however be pointed out, that the term inside the natural logarithm in Equations (A.3) and (A.4) is linearly dependent of the net reaction rate (i.e. current density), which means that the error of this approximation increases exponentially when the net reaction rate (i.e. current density) approaches zero. This inevitably means that activation losses cannot be well defined in these models, when operational points near open circuit voltage are considered, due to the error arising from the logarithmic function used in the Tafel equation. Furthermore, models [22,27] neglect anode activation losses on the anode side and therefore the entire Equation (A.4) is neglected.

The second category of reduced dimensionality electrochemical models, as presented in the Introduction, revolves around the Tafel equation extended by corrections for the low net reaction rate (i.e. current density) region. This approach is used in Refs. [31–33], where natural logarithm in the Tafel equation is a posteriori replaced with arcus sinus hyperbolicus as shown in Equations (A.3) and (A.4). In addition, these models also entirely neglect anode activation losses and anode kinetics. Taking into account these approximation, the equation equivalent of the one presented in Refs. [31–33] is obtained with Equation (A.5). A posteriori replacement of the logarithm in the Tafel equation with arcus sinus hyperbolicus successfully addresses the problem of addressing activation losses, when operational points near open circuit voltage are considered.

2.3. Consistent treatment of forward and backward reactions in BV

Derivation of the 0D TC FC electrochemical model proposed in the scope of this paper, relies on a mathematically consistent use of the sinus hyperbolicus definition on the BV equation. This can be applied assuming that $\alpha_c = 0.5$ and $\alpha_a = 0.5$. This results in an equation which is equivalent to the BV one and is valid over all current density regions. Consequentially the derivation stays thermodynamically consistent, however it losses a bit of generality, since the charge transfer coefficients can be fixed at 0.5 only, for so called symmetric reactions. For the anode side, this is in good agreement with experiments, whereas for the cathode side some references report deviations from these values, e.g. Ref. [34]. Thereby, it is reasonable to incorporate the proposed procedure by using an exponential definition of sinus hyperbolicus as:

$$e^{-\frac{\alpha_c e_0 Z_c \eta_c}{k_B T}} - e^{\frac{(1-\alpha_c) e_0 Z_c \eta_c}{k_B T}} = 2\sinh\left(-\frac{e_0 Z_c \eta_c}{k_B T} \right), \quad (19)$$

which gives, when used in Equation (17), the following expression:

$$j_c = j^c_0 \cdot e^{-\frac{E^c_0}{k_B T}} (\tilde{C}_{O_2})^{0.5} (\tilde{C}_{H_2O}) 2\sinh\left(-\frac{e_0 Z_c \eta_c}{k_B T} \right), \quad (20)$$

where E^c_0 is defined as:

$$E^c_0 = A_0 + \alpha_c \Delta g^0_c, \quad (21)$$

and j^c_0 as:

$$j^c_0 = e^{-\frac{\alpha_c \Delta s_c (T - T^0)}{k_B T}} e^{-\alpha_c \cdot \ln\left(\frac{k^*_{RDC}}{k_{OXC}}\right)} k^*_{RDC}. \quad (22)$$

Obtained expression presented in Equation (20) clearly exposes the difference between positioning of individual terms in expression for overvoltage given in Equation (A.5). Comparing obtained expression presented Equation (20) – obtained via consistent derivation with sinh from Butler-Volmer equation in case of symmetrical transfer coefficients and Equation (A.5) – obtained via introduction of sinh in ad hoc manner to replace natural logarithm clearly shows difference in positioning of individual terms. Even though both of the approaches solve the problem of larger errors in low current density regions, mathematical consistent basis enables easier parametrisation of the model and refines model performance as will be shown in the scope of this paper.

It is useful to point out that the obtained expression presented in Equation (20) give a net rate of the reaction on the cathode side, which is analogous to the expression for the current density presented if the aforementioned equations are multiplied with the factor $\frac{ZF}{S}$, where Z is number of electrons transferred in the electrochemical reaction, F is Faraday constant and S is surface area of FC. Similarly can be also done for net current of the cathode, when Equation (20) is multiplied with the factor ZF.

$$I_c = I^c_0 \cdot e^{-\frac{E^c_0}{k_B T}} (\tilde{C}_{O_2})^{0.5} (\tilde{C}_{H_2O}) 2\sinh\left(-\frac{e_0 Z_c \eta_c}{k_B T} \right), \quad (23)$$

where the factor ZF is incorporated in the terms I_0^c.

To obtain expressions for the reaction kinetics overpotential, which are the last terms in Equation (4) left to be defined, Equation (23) has to be rearranged to obtain the expression for the cathode side:

$$\eta_c = -\frac{k_B T}{e_0 Z_c}\operatorname{arcsinh}\left(\frac{I_c}{2I_0^c}e^{\frac{E_0^c}{k_B T}}(\tilde{C}_{O_2})^{-0.5}(\tilde{C}_{H_2O})^{-1}\right). \tag{24}$$

From Equation (24) it is easy to figure out the differences in functional dependencies and locations of individual terms in comparison with electrochemical models from the second category of reduced dimensionality electrochemical models as defined in the Introduction. The differences between both approaches can easily be seen when comparing Equations (A.5) and (24).

Inserting expressions from Equation (24) together with Equation (15) and analogous expressions for U_a^{OC} and η_a into Equation (4), the final version of the equation for voltage can be obtained:

$$\begin{aligned} U = {} & \frac{k_B T}{e_0 Z_c}\ln\left((\tilde{C}_{H_2O})^{-2}(\tilde{C}_{O_2})\right) - \frac{k_B T}{e_0 Z_c}\ln\left((\tilde{C}_{H_2})^2\right) \\ & + \frac{\Delta g_c^0}{e_0 Z_c} + \frac{(T-T^0)\Delta s_c}{e_0 Z_c} + \frac{\Delta g_a^0}{e_0 Z_a} + \frac{(T-T^0)\Delta s_a}{e_0 Z_a} \\ & + \frac{k_B T}{e_0 Z_c}\ln\left(\frac{k^*_{RDC}k_{OXA}}{k_{OXC}k^*_{RDA}}\right) - RI \\ & - \frac{k_B T}{e_0 Z_c}\operatorname{arcsinh}\left(\frac{I}{2I_0^c}e^{\frac{E_0^c}{k_B T}}(\tilde{C}_{O_2})^{-0.5}(\tilde{C}_{H_2O})^{-1}\right) \\ & - \frac{k_B T}{e_0 Z_a}\operatorname{arcsinh}\left(\frac{I}{2I_0^a}e^{\frac{E_0^a}{k_B T}}(\tilde{C}_{H_2})^{-1}\right). \end{aligned} \tag{25}$$

2.4. Simplified 1D transport of gaseous species in the GDL

The derived ansatzes do not directly address concentration losses due to the transport of species in the GDL. However the concentration losses can be easily incorporated in Equation (25) via simplified model for transport of gaseous species in 1D as presented in Refs. [33,34]. Due to the importance of this step in the devising procedure of the model it is presented in detail in Supplementary material. The idea behind simplified transport model is that concentration of reactants on the catalyst layer ($C_{r_{CL}}$) can be calculated using ratio between limiting current (I_L) and current density (I) as following:

$$C_{r_{CL}} = C_{r_{chan}}\left(1 - \frac{I}{I_L}\right), \tag{26}$$

where $C_{r_{chan}}$ is the concentration of reactants in channel and limiting current can be written as a function of constants and physical properties of the GDL:

$$I_L = ZFSD_{rr}\frac{C_{r_{chan}}}{\delta_{GDL}}, \tag{27}$$

If the obtained relation for concentration on the GDL – catalyst layer interface is inserted in Equation (25) for FC potential, the following equation is obtained, which has simplified transport of species influencing concentration losses incorporated:

$$\begin{aligned} U = {} & \frac{k_B T}{e_0 Z_c}\ln\left(\left(\tilde{C}_{H_2O}\left(1+\frac{I}{I_{L_c}}\right)\right)^{-2}\left(\tilde{C}_{O_2}\left(1-\frac{I}{I_{L_c}}\right)\right)\right) \\ & - \frac{k_B T}{e_0 Z_a}\ln\left(\left(\tilde{C}_{H_2}\left(1-\frac{I}{I_{L_a}}\right)\right)^2\right) + \frac{k_B T}{e_0 Z}\ln\left(\frac{k^*_{RDC}k_{OXA}}{k_{OXC}k^*_{RDA}}\right) \\ & + \frac{\Delta g_c^0}{e_0 Z_c} + \frac{(T-T^0)\Delta s_c}{e_0 Z_c} + \frac{\Delta g_a^0}{e_0 Z_a} + \frac{(T-T^0)\Delta s_a}{e_0 Z_a} - RI \\ & - \frac{k_B T}{e_0 Z_c}\operatorname{arcsinh}\left(\frac{I}{2I_0^c}e^{\frac{E_0^c}{k_B T}}\left(\tilde{C}_{O_2}\left(1-\frac{I}{I_{L_c}}\right)\right)^{-0.5}\left(\tilde{C}_{H_2O}\left(1+\frac{I}{I_{L_c}}\right)\right)^{-1}\right) \\ & - \frac{k_B T}{e_0 Z_a}\operatorname{arcsinh}\left(\frac{I}{2I_0^a}e^{\frac{E_0^a}{k_B T}}\left(\tilde{C}_{H_2}\left(1-\frac{I}{I_{L_a}}\right)\right)^{-1}\right). \end{aligned} \tag{28}$$

2.5. Simplified 1D transport of gaseous species along the channel

Stoichiometric ratio has a profound effect on the gaseous species concentration along the channel and thus performance of the FC. To assure sufficient modelling accuracy, while not sacrificing computational speed needed in control applications, analytical solution of convection diffusion equation has been sought:

$$\frac{\partial c}{\partial t} = \nabla(D\nabla c) - \nabla(vc) + Sr, \tag{29}$$

where c is the concentration of individual species in the channel, t is time, D is diffusive coefficient, v is speed of gases in the channel and Sr is the source term, which is $Sr < 0$ for oxygen and hydrogen and $Sr > 0$ for gaseous water. Strictly speaking source term is concentration and position dependent (Equation (17)). To assure attainment of analytical solution of Equation (29) several assumptions, which are all in line with assumptions introduced in previous sections, are taken into consideration. Namely the following: diffusion coefficient is taken as a constant, velocity field along the channel is approximately uniform ($\nabla v = 0$) and effects of diffusive transport are for at least an order of magnitude less pronounce than those of convective, therefore $\nabla^2 c \approx 0$. This way reduced version of Equation (29) can be written as:

$$\frac{\partial c}{\partial t} = -v\nabla c + Sr, \tag{30}$$

and the 1D version of the Equation can be written as:

$$\frac{\partial c(y)}{\partial t} = -v_y\frac{\partial c(y)}{\partial y} + Sr(y), \tag{31}$$

where y axis is directed along side the channel and $Sr(y)$ is:

$$Sr(y) = e^{-\frac{A_0}{k_B T}}e^{-\frac{\alpha_c \Delta s_c^0}{k_B T}}e^{-\frac{\alpha_c \Delta s_c}{k_B T}\left(T-T^0\right)}e^{-\alpha_c \cdot \ln\left(\frac{k^*_{RDC}}{k_{OXC}}\right)}(\tilde{C}_{O_2}(y))^{0.5}\cdot\tilde{C}_{H_2O}k^*_{RDC}\left(e^{-\frac{\alpha_c e_0 Z_c \eta_c}{k_B T}} - e^{\frac{(1-\alpha_c)e_0 Z_c \eta_c}{k_B T}}\right). \tag{32}$$

Obtained expression for source term can be divided into two parts, part dependent of position (y) along the channel and part which is not (γ).

$$Sr(y) = \gamma \cdot (\tilde{C}_{O_2}(y))^{0.5} \tag{33}$$

Analytical solution of this set of equations can be found:

$$\tilde{C}_{O_2}(y,t) = 0.25k_1\left(\frac{(v_{c_i n}ZFh)t - y}{(v_{c_i n}ZFh)}\right)^2 + \frac{I}{\left(\frac{ZFD_{rr}}{\delta_{GDL}}\right)} - \frac{0.5\gamma y k_1\left(\frac{(v_{c_i n}ZFh)t-y}{(v_{c_i n}ZFh)}\right)}{(v_{c_i n}ZFh)} + \frac{0.25\gamma^2 y^2}{(v_{c_i n}ZFh)^2} \tag{34}$$

where k_1 is the constant which can be obtained for each individual boundary condition $\tilde{C}_{O_2}(0,t)$ and h is the hight of the channel. The solution of the problem is even simpler when steady state solution is sought. The result for the steady state set of equations with boundary condition set as $\tilde{C}_{O_2}(0) = c_{in}$, where c_{in} is the inlet concentration of the oxygen, can be written as:

$$\tilde{C}_{O_2}(y) = c_{in} + \frac{0.25\gamma^2 y^2}{(v_{c_i n}ZFh)^2} - \frac{\gamma y (v_{c_i n}ZFh)\sqrt{c_{in}\left(\frac{ZFD_{rr}}{\delta_{GDL}}\right)} - I}{(v_{c_i n}ZFh)^2\sqrt{\left(\frac{ZFD_{rr}}{\delta_{GDL}}\right)}}. \tag{35}$$

Developed simplified analytical 1D model for transport of gaseous species along the channel meets the necessary requirement of ease of computation, while coupled with quasi-1D electrochemical model offers also insight in effect of decreasing concentration profile of oxygen and hydrogen on the cathode and anode side, respectively, on the performance of the FC.

3. Methodology and framework for in-depth electrochemical model assessment

The obtained thermodynamically consistent derivation of the model ensures a consistent analytically derived expression for the polarisation curve throughout all current density regions. To successfully reduce calibration times of the TC FC electrochemical model and assure a high quality fit, both of which are crucial for enhanced applicability of the model, this section presents all necessary steps for the determination of the optimal set of calibration parameters.

3.1. Determining set of calibration parameters

To determine the initial set of calibration parameters, the newly derived Equation (28) for the TC FC electrochemical model was analysed. First, inputs based on operational conditions and known values of physical constants were determined and inserted into the expression. This was instrumental for assuring both high generality and good prediction capability of the parametrised model on one side and avoiding over-fitting on the other. The latter can easily reduce generality of the derived electrochemical model and increase models precision in only one operational point. Therefore, values of F, k_B, e_0, Z_c, Z_a, Δg_c^0, Δg_a^0, T^0, Δs_c and Δs_a, which are all literature known constants were set and α_c, α_a were fixed to 0.5, due to introduction of sinus hyperbolicus. On the other hand, current, temperature and concentrations are operational parameters.

$$U = \frac{k_B T}{e_0 Z_c}\ln\left(\left(\tilde{C}_{H_2O}\left(1+\frac{I}{I_{L_c}}\right)\right)^{-2}\left(\tilde{C}_{O_2}\left(1-\frac{I}{I_{L_c}}\right)\right)\right) - \frac{k_B T}{e_0 Z_a}\ln\left(\left(\tilde{C}_{H_2}\left(1-\frac{I}{I_{L_a}}\right)\right)^2\right) + \frac{k_B T}{e_0 Z}\ln\left(\frac{k^*_{RDC}k_{OXA}}{k_{OXC}k^*_{RDA}}\right) + \frac{\Delta g_c^0}{e_0 Z_c} + \frac{(T-T^0)\Delta s_c}{e_0 Z_c} + \frac{\Delta g_a^0}{e_0 Z_a} + \frac{(T-T^0)\Delta s_a}{e_0 Z_a} - RI - \frac{k_B T}{e_0 Z_c}\operatorname{arcsinh}\left(\frac{I}{2I_0^c e^{\frac{E_0^c}{k_B T}}}\left(\tilde{C}_{O_2}\left(1-\frac{I}{I_{L_c}}\right)\right)^{-0.5}\left(\tilde{C}_{H_2O}\left(1+\frac{I}{I_{L_c}}\right)\right)^{-1}\right) - \frac{k_B T}{e_0 Z_a}\operatorname{arcsinh}\left(\frac{I}{2I_0^a e^{\frac{E_0^a}{k_B T}}}\left(\tilde{C}_{H_2}\left(1-\frac{I}{I_{L_a}}\right)\right)^{-1}\right) \tag{36}$$

The reaction rates on the cathode and anode side (k^*_{RDC}, k_{OXA}, k_{OXC} and k^*_{RDA}) and the resistance (R) are calibration parameters of the model, whereas limiting currents (I_{L_a}, I_{L_c}) and intrinsic exchange current density on the cathode and anode side (I_0^c, I_0^a) are functions of other calibration parameters. The limiting current for anode side is defined as:

$$I_{L_a} = Z_a FSD_{eff_a}\frac{C_{r_a}}{\delta_{GDL_a}} = Z_a FC_{r_a}CD_a, \tag{37}$$

where only the combined diffusivity parameter CD_a is being calibrated and not the effective diffusivity D_{eff_a} and width of GDL δ_{GDL_a} separately, since this pair of calibration parameters cannot be uniquely determined. Linear dependency between both terms can also be observed on the cathode side, where only CD_c is being calibrated:

$$I_{L_c} = Z_c FSD_{eff_c}\frac{C_{r_c}}{\delta_{GDL}} = Z_c FC_{r_c}CD_c. \tag{38}$$

Intrinsic exchange current depends highly on the physical ansatz:

$$I_0^c = S\cdot e^{-\frac{\alpha_c \Delta s_c\left(T-T^0\right)}{k_B T}} e^{-\alpha_c \cdot \ln\left(\frac{k^*_{RDC}}{k_{OXC}}\right)} k^*_{RDC}. \tag{39}$$

In the equation above it is necessary to calibrate only the reaction rates on the anode and cathode side, all the other terms are either physical constants or variables such as temperature. A similar expression can be obtained for the anode side as well:

$$I_0^a = S\cdot e^{-\frac{\alpha_a \Delta s_a\left(T-T^0\right)}{k_B T}} e^{-\alpha_a \cdot \ln\left(\frac{k_{OXA}}{k^*_{RDA}}\right)} k_{OXA}. \tag{40}$$

Based on functional dependencies presented in the equations above, a set of 9 calibration parameters is determined, namely: E_{0_c}, E_{0_a}, k^*_{RDC}, k_{OXC}, k^*_{RDA}, k_{OXA}, R, CD_c, CD_a.

3.2. Calibration procedure

The obtained set of calibration parameters presents a basis for the calibration procedure, which is based on the process of minimization of the penalty function value. Thus fitting the model output to the experimental data, with physically plausible constraints introduced on the calibration parameters (calibration parameters have physically plausible values). Based on the model type, the calibration procedure was run with global and local optimization algorithms, namely gradient ('*fminsearch*' [37]) and genetic optimization algorithms ('*ga*' [37]). The latter is a metaheuristic method for solving both constrained and unconstrained optimization problems that is inspired by the process of natural selection. Usually it works well when the parameter space is large, due to the fact that it is less prone to getting stuck in local minima of the penalty function, compared to the gradient algorithm, however it is computationally more demanding and therefore, slower. To bypass this problem after some iterations the genetic algorithm was exchanged

with a gradient one, which is a much faster approach using gradient descent.

3.3. Assessment of reduction of calibration parameters set

A balance between model calibration parameter identifiability, accuracy of the model, and computational time to achieve optimized values of calibration parameters is crucial to ensuring that the model can exhibit good extrapolation capabilities and robustness. Therefore, to comply with this criteria, an assessment of the initial calibration parameter set has to performed. Possible model reductions are analysed from both a mathematical and physical standpoint. To confirm the proposed knowledge based reductions, whether mathematical or physical, especially in borderline cases, parameter sensitivity analysis is performed.

3.4. Mathematical assessment

First, the set of initial calibration parameters has to be analysed to determine a possible linearly dependent set of calibration parameters. One of these problematic instances has already been addressed in Equations (37) and (38), where obvious linearly dependant parameters of effective diffusivity and width of GDL were lumped together to form a single calibration parameter. Detailed inspection of the obtained Equations (36), (39) and (40) reveals their dependence on k^*_{RDC}, k_{OXC} on the cathode side and k^*_{RDA}, k_{OXA} on the anode side. It is clear that based solely on Equation (36) where the term:

$$\frac{k_B T}{e_0 Z} \ln\left(\frac{k^*_{RDC} k_{OXA}}{k_{OXC} k^*_{RDA}}\right) \tag{41}$$

can be found, these calibration parameters cannot be uniquely determined, due to the fact that any change in the value of one of the parameters would not result in a change of voltage, if the value of other parameter would proportionally change. However, due to the functional dependency in Equations (39) and (40), they cannot be easily lumped together without affecting the pure mechanistical basis of the model. That also means that a theoretical ideal data set exists, based on which individual parameters could be determined. This challenge calls for

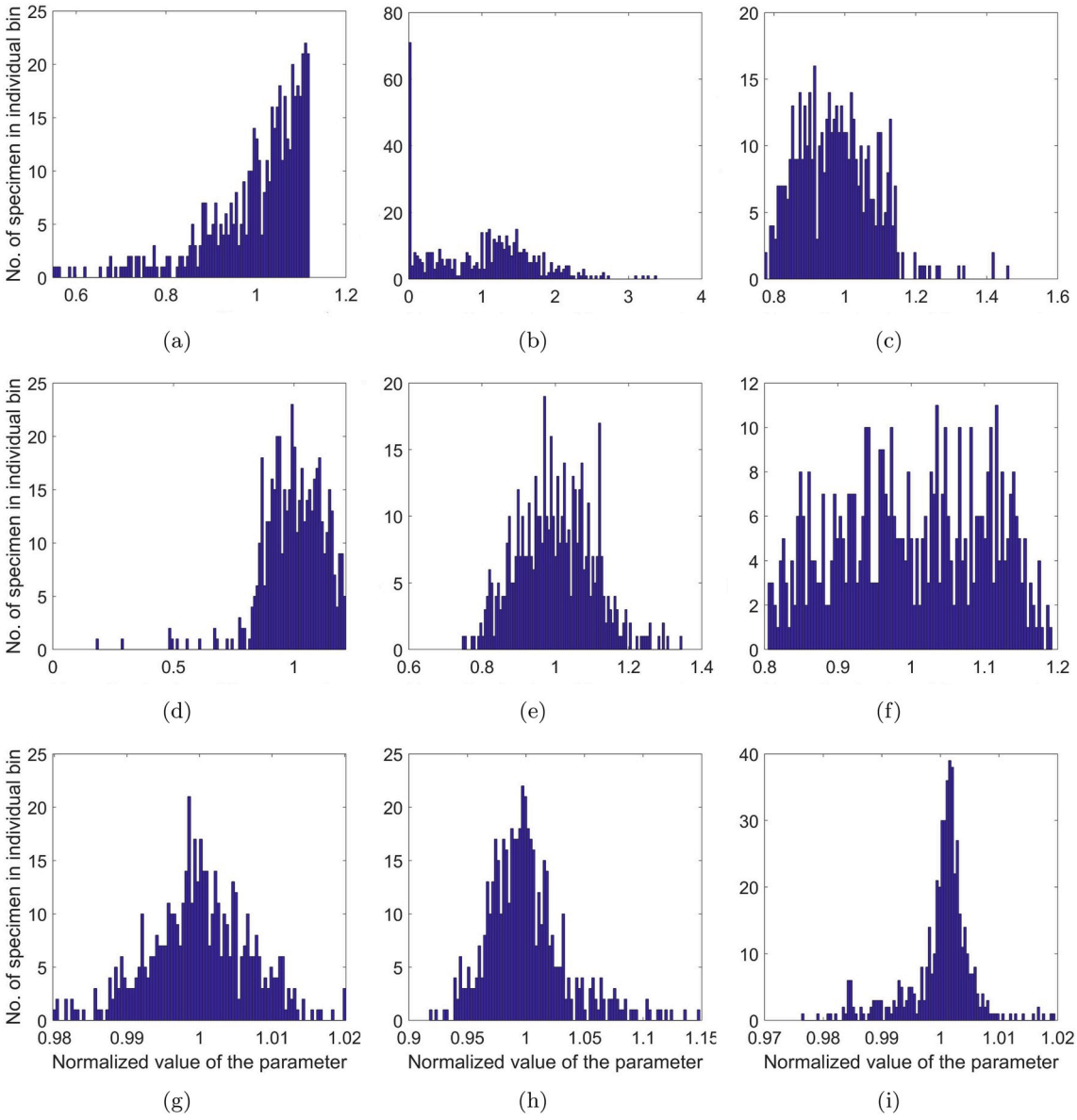

Fig. 2. Spread of the normalized value of calibration parameters for TC FC electrochemical model, namely: (a) - E_{0_c}, (b) - E_{0_a}, (c) - k^*_{RDC}, (d) - k_{OXC}, (e) - k^*_{RDA}, (f) - k_{OXA}, (g) - R, (h) - CD_c, (i) - CD_a.

parameter sensitivity analysis to ensure an appropriate replacement of the calibration parameters.

3.5. Parameter sensitivity

To confirm the proposed reductions, especially in borderline cases such as those presented in the Mathematical assessment, parameter sensitivity is invaluable. Parameter sensitivity analysis can be performed with various methods i.e. with the Fisher information or with Fourier Amplitude Sensitivity Test. In this paper it was performed via analysis of the calibration parameter values obtained in a Monte Carlo like simulation procedure that included a genetic algorithm. To test this aspect of the model, a genetic optimization algorithm ('*ga*' [37]) was run for single and multiple polarisation curves 500 times with 1000 generations each with a population size of 200 and InitialPopulationRange determined as $\pm 0.2\theta$. The initial vector θ consisted of an already optimized set of parameters obtained from a calibration procedure on the TC FC electrochemical model with the initial 9 calibration parameters. In this kind of analysis, each individual parameter has a certain amount of spread as shown in Fig. 7d. Theoretically speaking, a lower spread of a parameter's value is directly correlated with the possibility of it being uniquely determined on the present data set. The obtained spreads of parameters are presented in Fig. 2. Figure reveals that E_{0_c}, k^*_{RDC}, k_{OXA} and R are more readily determined than for example k^*_{RDA}, which shows a totally random spread.

3.6. Physical assessment

A purely physical assessment of individual calibration parameters is invaluable, especially when it comes to determining the more influential parameters in cases where parameter sensitivity analysis and a mathematical approach to model reduction fail to present an unquestionable answer. One of these examples is the widely known fact that kinetics on the cathode side are rate limiting and therefore, have more influence on the overall performance of the FC. This is why some models completely neglect the anode kinetics [22,27,32,33], which starts to affect model generality, predictiveness, and accuracy and should therefore be avoided. Furthermore, due to the fact that anode side has an effect of up to several 10 mV on the polarisation curve, it is beneficial to leave the effects of the anode kinetics in the model. Additionally, performed parameter sensitivity shows (Fig. 2) that for example CD_a can be very well determined based on the calibration of the model on polarisation curve, therefore its effects are distinguishable from the effects of R or CD_c. However, in cases where the amount of data for the calibration of parameters is immensely scarce, it can still be beneficial, since it is highly likely that the obtained cathode parameters will be better defined as a direct consequence of the reduction.

Due to the fact that anodic kinetics are at least for an order of magnitude less influential for performance of FC under normal operating conditions, it can be easily explained that the reduction rate on the anode side, therefore reaction rate of the reaction in backward direction, is one of the less influential parameters on the anode and consequentially on the performance of FC as a whole. Therefore, calibration parameters describing the reduction rate on the anode side are highly unlikely to be determined, even if the data set used for calibration is designed solely with the aim of unravelling anode kinetics. This is fully confirmed with the results of parameter sensitivity analysis presented in Fig. 2.

3.6.1. Reduction of calibration parameter set for normal operational conditions

Parameters which have a totally random spread, such as aforementioned k^*_{RDA}, cannot be uniquely determined, or their influence on the data set used for the calibration procedure is extremely low. Based on the observed totally random spread in Fig. 2, the proposed reduction of the calibration parameters as discussed in Section 3.4, which define reaction rates by being lumped together, is meaningful. Therefore, the proposed reduction can be written as:

$$e^{-\alpha_c \cdot \ln\left(\frac{k^*_{RDC}}{k_{OXC}}\right)} k^*_{RDC} \rightarrow K_c. \tag{42}$$

$$e^{-\alpha_a \cdot \ln\left(\frac{k_{OXA}}{k^*_{RDA}}\right)} k_{OXA} \rightarrow K_a. \tag{43}$$

However, this reduction of parameter space cannot be easily lumped together due to the term (41) with four reaction rates in Equation (36). Therefore, this approximation has a small influence on the TC FC electrochemical model due to the fact that the term on the left side of the expression:

$$\frac{k_B T}{e_0 Z} \ln\left(\frac{k^*_{RDC} k_{OXA}}{k_{OXC} k^*_{RDA}}\right) \rightarrow 0, \tag{44}$$

cannot be determined. This is reasoned by the fact that the parameters presented in this term cannot be substituted with the newly chosen set of calibration parameters. However, this has a negligible effect on the output voltage from the TC FC electrochemical model, since the magnitude of the neglected term is 10^{-4} V at its largest for TC FC electrochemical model with all 9 calibration parameters. Therefore, it can be set to 0, with a negligible loss of model generality. Nevertheless, it has to be pointed out that in operational conditions where the kinetics on both the anode and cathode extremely differ from normal operation conditions e.g. in the case of fuel starvation, this could change. Since these kind of operation conditions can be largely avoided even during loading-up [38–40], the aforementioned possibility is minor.

With the newly determined set of two parameters K_c and K_a, the intrinsic exchange current density can be written as:

$$I^c_0 = S \cdot e^{-\frac{\alpha_c \Delta s_c \left(T - T^0\right)}{k_B T}} \cdot K_c, \tag{45}$$

$$I^a_0 = S \cdot e^{-\frac{\alpha_a \Delta s_a \left(T - T^0\right)}{k_B T}} \cdot K_a. \tag{46}$$

Based on the new set of calibration parameters and the reduction of the electrochemical model, the electrochemical ansatz [36] can now be rewritten as:

This way the reduced set of calibration parameters consists of: E_{0_c}, E_{0_a}, K_c, K_a, R, CD_c, CD_a. Their functional influence on the voltage of FC,

$$U = \frac{k_B T}{e_0 Z_c} \ln\left(\left(\tilde{C}_{H_2O}\left(1 + \frac{I}{I_{L_c}}\right)\right)^{-2}\left(\tilde{C}_{O_2}\left(1 - \frac{I}{I_{L_c}}\right)\right)\right) - \frac{k_B T}{e_0 Z_a} \ln\left(\left(\tilde{C}_{H_2}\left(1 - \frac{I}{I_{L_a}}\right)\right)^{2}\right) + \frac{\Delta g^0_c}{e_0 Z_c} + \frac{\left(T - T^0\right)\Delta s_c}{e_0 Z_c} + \frac{\Delta g^0_a}{e_0 Z_a} + \frac{\left(T - T^0\right)\Delta s_a}{e_0 Z_a}$$
$$- RI - \frac{k_B T}{e_0 Z_c} \operatorname{arcsinh}\left(\frac{I}{2I^c_0} e^{\frac{E^c_0}{k_B T}}\left(\tilde{C}_{O_2}\left(1 - \frac{I}{I_{L_c}}\right)\right)^{-0.5}\left(\tilde{C}_{H_2O}\left(1 + \frac{I}{I_{L_c}}\right)\right)^{-1}\right) - \frac{k_B T}{e_0 Z_a} \operatorname{arcsinh}\left(\frac{I}{2I^a_0} e^{\frac{E^a_0}{k_B T}}\left(\tilde{C}_{H_2}\left(1 - \frac{I}{I_{L_a}}\right)\right)^{-1}\right) \tag{47}$$

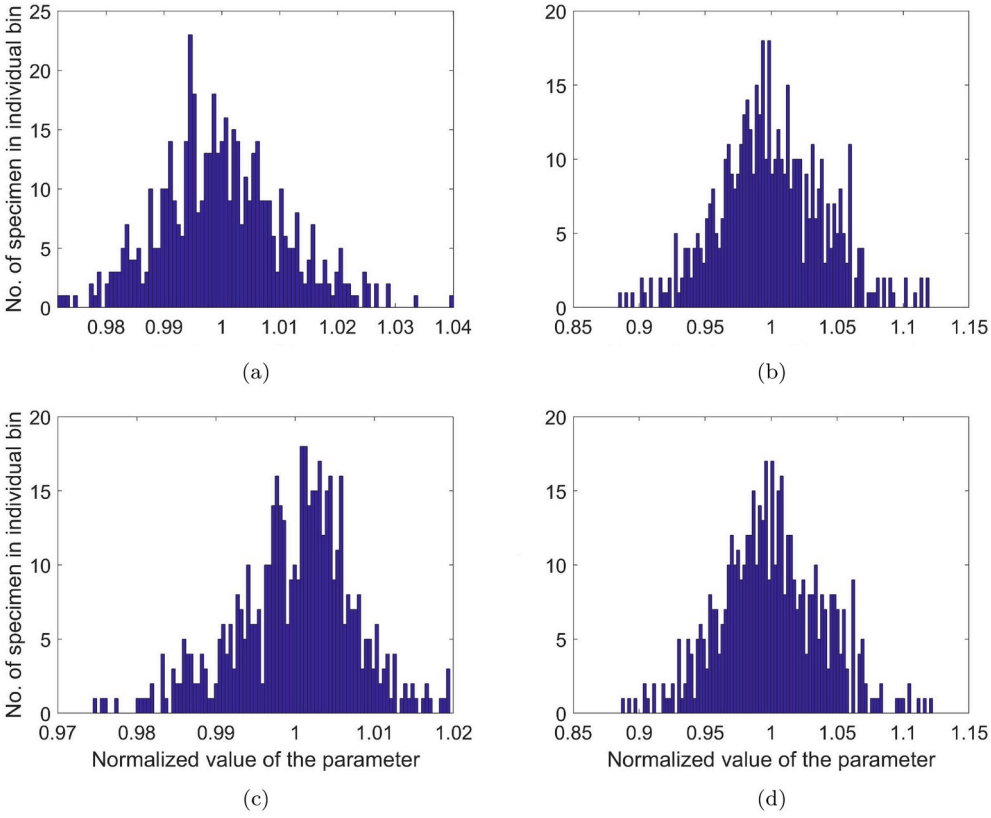

Fig. 3. Spread of the normalized values of K_c - (a), K_a - (b), $\widetilde{I}_0^c$ - (c) and $\widetilde{I}_0^a$ - (d) for the TC FC electrochemical model.

can be easily seen only for the activation energies on the cathode and anode side (E_{0_c}, E_{0_a}) and the resistance (R) from Equation (47). Whereas, intrinsic exchange current density on the cathode and anode side (I_0^a, I_0^c) are functions of two calibration parameters K_a and K_c as presented in Equations (46) and (45). Similarly, limiting currents (I_{L_a}, I_{L_c}) are functions of two calibration parameters CD_a and CD_c as presented in Equations (37) and (38).

The direct effect of a reduced set of calibration parameters can be seen in Fig. 3a and b, where the spread of the normalized values of K_c and K_a is now smaller compared to those of k^*_{RDC}, k_{OXC}, k^*_{RDA}, k_{OXA} and their distribution resembles the Gaussian one. Therefore, the result of parameter sensitivity analysis confirm the reasonableness of the proposed reduction in Sections 3.4 and 3.6. From this point onward all results presented in the scope of this paper are obtained with this set of calibration parameters unless stated otherwise.

3.6.2. *Reduction of calibration parameter set for near isothermal operation*

Further reduction of calibration parameter set is possible, if isothermality of each individual electrode is assumed. The possible reduction comes from lumping together E_{0_c} and K_c for the cathode side and E_{0_a} and K_a for the anode side in Equation (47), which are, in the case of near isothermal operation, linearly dependant on each other. This reasoning is in line with the theoretical foundations presented in Sections 3.4 and 3.6 and confirmed by Fig. 2, where a high spread of calibration parameters describing activation energies on the cathode and anode side (E_{0_c} and E_{0_a}) are observed. The proposed reduction is presented in the following two equations:

$$I_0^c = S \cdot \mathrm{e}^{-\frac{\alpha_c \Delta s_c \left(T-T^0\right)}{k_B T}} \cdot K_c \cdot \mathrm{e}^{\frac{-E_0^c}{k_B T}} = S \cdot \mathrm{e}^{-\frac{\alpha_c \Delta s_c \left(T-T^0\right)}{k_B T}} \cdot \widetilde{I}_0^c, \tag{48}$$

$$I_0^a = S \cdot \mathrm{e}^{-\frac{\alpha_a \Delta s_a \left(T-T^0\right)}{k_B T}} \cdot K_a \cdot \mathrm{e}^{\frac{-E_0^a}{k_B T}} = S \cdot \mathrm{e}^{-\frac{\alpha_a \Delta s_a \left(T-T^0\right)}{k_B T}} \cdot \widetilde{I}_0^a. \tag{49}$$

Inserting the expressions for the newly determined calibration parameters $\widetilde{I}_0^a$ and $\widetilde{I}_0^c$ into Equation (47) results in:

$$\begin{aligned} U = {} & \frac{k_B T}{e_0 Z_c} \ln\left(\left(\tilde{C}_{H_2O}\left(1+\frac{I}{I_{L_c}}\right)\right)^{-2}\left(\tilde{C}_{O_2}\left(1-\frac{I}{I_{L_c}}\right)\right)\right) + \\ & -\frac{k_B T}{e_0 Z_a} \ln\left(\left(\tilde{C}_{H_2}\left(1-\frac{I}{I_{L_a}}\right)\right)^{2}\right) + \\ & +\frac{\Delta g_c^0}{e_0 Z_c} + \frac{(T-T^0)\Delta s_c}{e_0 Z_c} + \frac{\Delta g_a^0}{e_0 Z_a} + \frac{(T-T^0)\Delta s_a}{e_0 Z_a} - RI + \\ & -\frac{k_B T}{e_0 Z_c} \operatorname{arcsinh}\left(\frac{I_c}{2I_0^c}\left(\tilde{C}_{O_2}\left(1-\frac{I}{I_{L_c}}\right)\right)^{-0.5}\left(\tilde{C}_{H_2O}\left(1+\frac{I}{I_{L_c}}\right)\right)^{-1}\right) + \\ & -\frac{k_B T}{e_0 Z_a} \operatorname{arcsinh}\left(\frac{I_a}{2I_0^a}\left(\tilde{C}_{H_2}\left(1-\frac{I}{I_{L_a}}\right)\right)^{-1}\right) \end{aligned} \tag{50}$$

This way a second set of reduced calibration parameters can be written as: $\widetilde{I}_0^c$, $\widetilde{I}_0^a$, R, CD_c, CD_a. The spread of normalized values of $\widetilde{I}_0^c$ and $\widetilde{I}_0^a$ is in this case smaller compared to those of E_{0_c}, E_{0_a}, K_c, K_a and their distribution too resembles the Gaussian one as shown in Fig. 3c and d.

Furthermore, this reduced set of calibration parameters enables a direct correlation to the SoH parameters of the FC. Correlation between the electrochemical active surface area (ECSA) and the calibration parameters $\widetilde{I}_0^a$ and $\widetilde{I}_0^c$ is easily obtainable and a relative change in membrane conductivity can be directly correlated to the change in R values.

Table 1
Operating conditions of FC under which polarisation curves were obtained.

No.	λ_{an}	λ_{cat}	$p_{in_{an}}$ [bar]	$p_{in_{cat}}$ [bar]	RH_{an} [%]	RH_{cat} [%]	T [K]
1	1,3	1,8	1,013	1,013	0	80	343,15
2	1,3	1,7	1,4	1,4	0	80	346,15
3	1,3	1,7	2,0	2,0	0	80	347,15
4	1,3	1,7	2,5	2,5	0	80	349,15

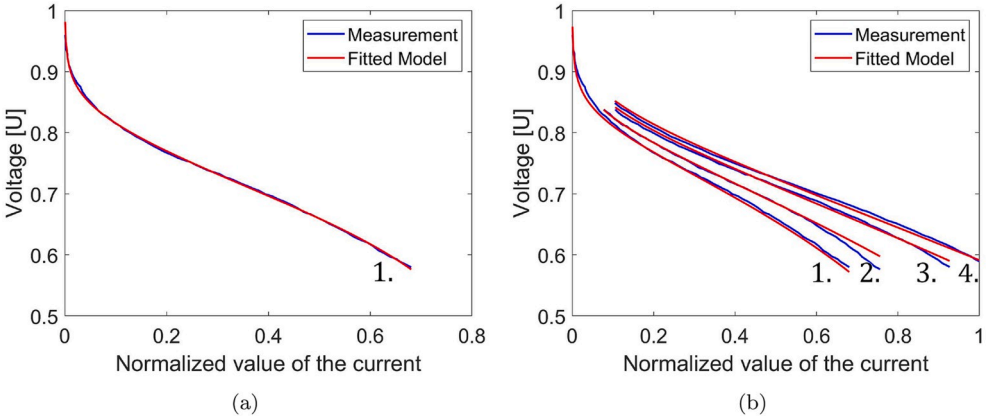

Fig. 4. Results of the calibrated model for single - (a) and multiple polarisation curves - (b).

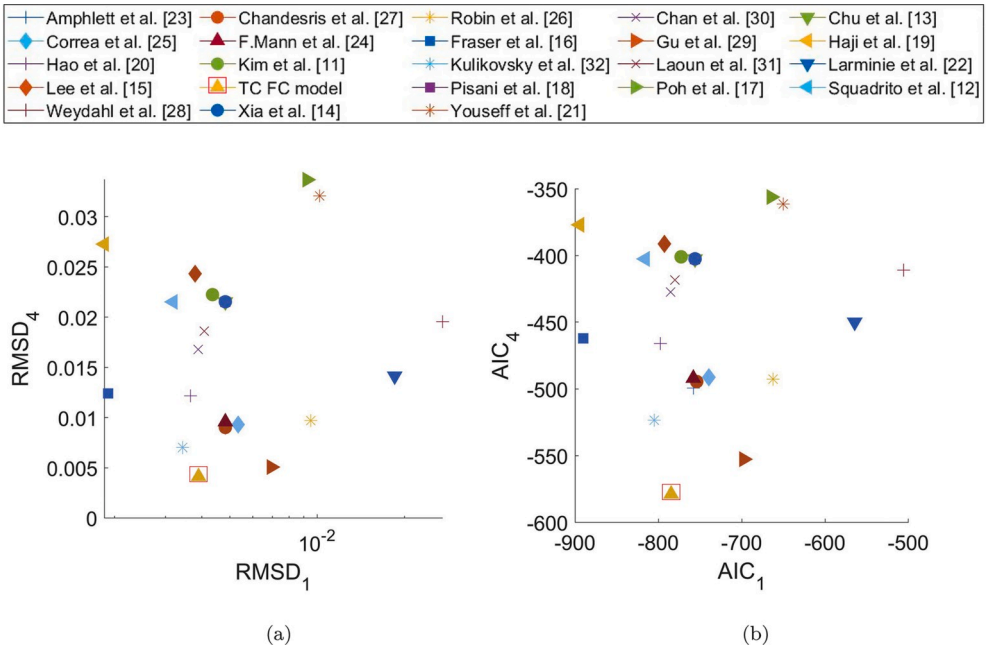

Fig. 5. Results obtained with a calibration performed on only one polarisation curve are presented on the x-axis, whereas results obtained with calibration performed on multiple polarisation curves are presented on y-axis for different information criteria ((a) - RMSD and (b) - AIC).

Finally, a change in the values of the calibration parameters CD_c, CD_a can directly be attributed to a change in the hydrophobicity of the GDL.

4. Results and discussions

Thermodynamically sound derivation of electrochemical model, determination of calibration parameters and parameter sensitivity assessment with the aim of proposing feasible and meaningful model reductions, are just three of several crucial steps in the process, which assures that the newly obtained model will have highest possible prediction capability and generality. It is equally important to determine the most suitable optimization algorithm to assess the capabilities of the model at hand and to determine its convergence speed.

4.1. Fitting to experimental data

Fit assessment and model calibration were performed with gradient (*'fminsearch'* [37]) and genetic optimization algorithms (*'ga'* [37]) on the experimentally obtained data of the FC stack. Data consisted of 4 individual polarisation curves which were obtained at different operating conditions as defined in Table 1.

Due to the fact that the FC temperature is not constant for the data set at hand, the TC FC electrochemical model with 7 calibration parameters (presented in Section 3.6.1) was used. Using isothermal version of the TC FC electrochemical model with 5 calibration parameters (presented in Section 3.6.2) would in this case result in increased calibration error by 2% for $\tilde{I}_0^a$ and $\tilde{I}_0^c$ in comparison to TC FC electrochemical model with 7 calibration parameters, due to different operation temperatures of FC during measurement of multiple polarisation curves.

The results of the calibrated TC FC electrochemical model show very good agreement between the model and experiment for single and multiple experiments calibrated at once, which can be seen from Fig. 4. To assess model robustness and extrapolation capabilities it was benchmarked with state-of-the-art computationally fast electrochemical models and models widely used in literature.

4.2. Calibration results for single and multiple experiments and comparison with other models

An overview of the literature showed that more than 20 different fast electrochemical models are used in applications when a low computational burden is needed. Their differentiation in two major categories was shown in the Introduction and differences between their leading equations was addressed in Section 2.2. Due to the fact that each of the presented models uses at least one simplification, a comparison of these electrochemical models with the TC FC electrochemical model is performed. To fulfil this goal 23 different electrochemical models were coded into the devised framework, which was used for calibration procedures in the beginning with the model proposed in this paper.

A crucial step in the analysis of the electrochemical model is an appropriate assessment of its fit quality. Due to the fact that several different information criteria exist in literature, all of which are used for an assessment of the obtained fit quality, the calibration procedure for each of the aforementioned electrochemical models on single and multiple polarisation curves was run with root mean square deviation (RMSD) as error assessment criteria and Akaike information criterion (AIC) as an estimator of the relative quality of models for a given set of data. RMSD is defined as:

$$\mathrm{RMSD} = \sqrt{\frac{\sum_{i=1}^{n}(y_i - f(x_i))^2}{n}} \tag{51}$$

where n is size of data set, y_i and $f(x_i)$. Whereas, AIC information criterion is defined as:

$$\mathrm{AIC} = n \cdot \ln\left(\frac{\sum_{i=1}^{n}(y_i - f(x_i))^2}{n}\right) + 2k \tag{52}$$

where $2k$ is penalising term with k being number of calibration parameters. The results obtained by AIC are presented in Fig. 5.

An ideal model would always, regardless of the criterion used, have the same value of error for both single and multiple experiments, and would assuming that the produced data would not have any measurement error or noise, yield in the case of error assessment criteria result 0. However, this is generally not the case. Models which are empirically based [11–20], i.e. data driven models, are in general very well behaved when only one operational point is being calibrated, however they perform poorly when describing the experimental data where multiple operational points are being calibrated. This property of data driven models is clearly visible in Fig. 5.

However, it should be pointed out that by over-fitting or fitting too many calibration parameters, excellent results for a given data set can always be obtained. To satisfactorily take into account the number of

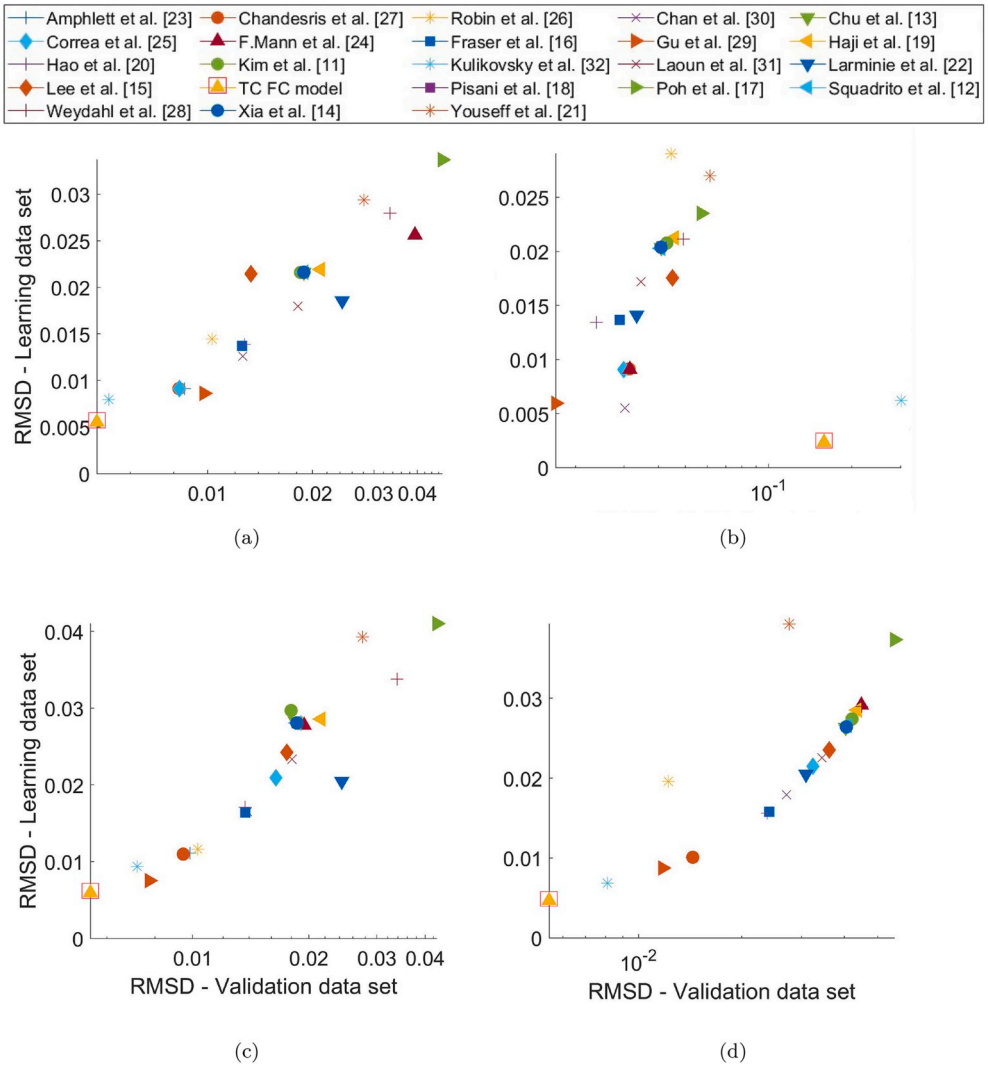

Fig. 6. RMSD values for: a) first extrapolation validation, b) second extrapolation validation, c) first interpolation validation, d) second interpolation validation.

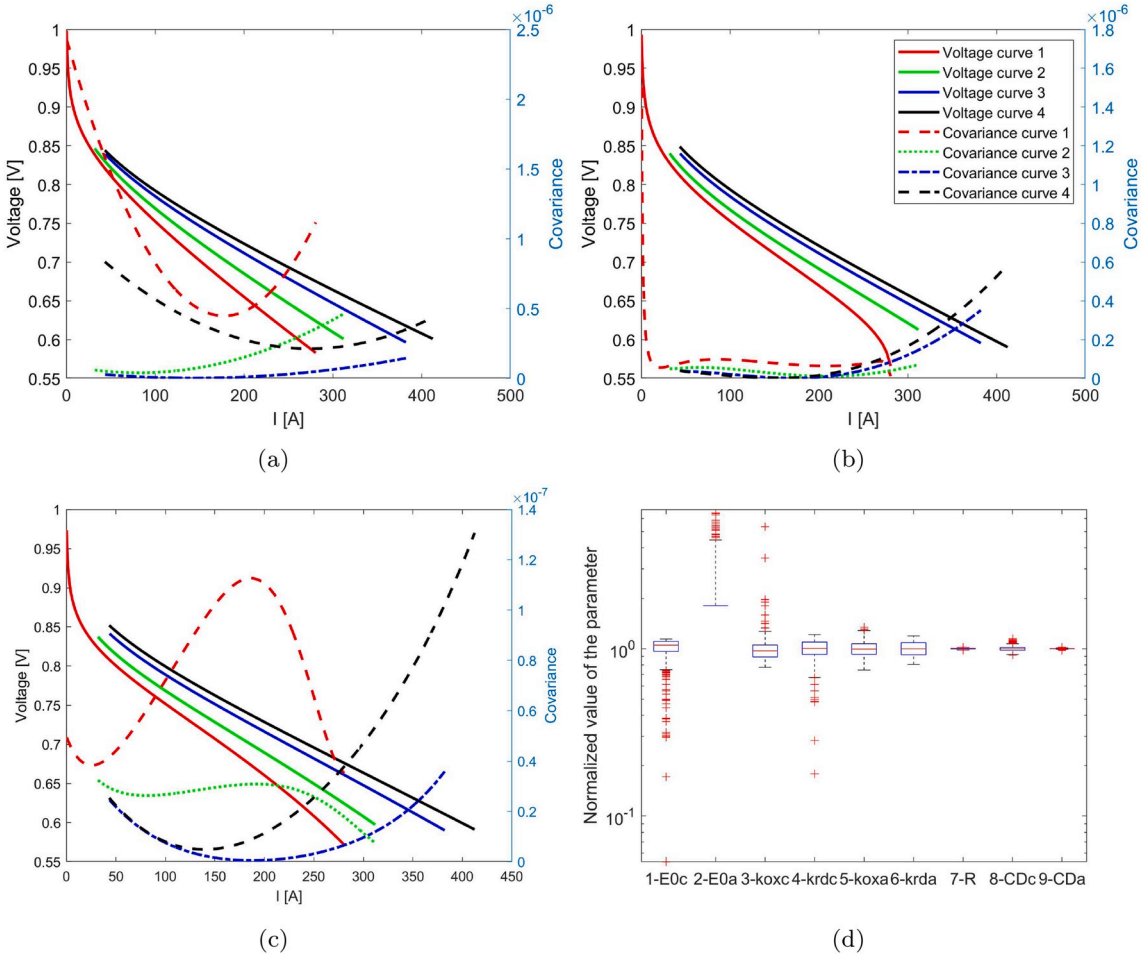

Fig. 7. Covariance of the calculated voltage for 500 sets of obtained calibration parameters for Gu's [29] (a), Kulikovsky's model [32] (b) and the TC electrochemical model (c). Figure (d) shows the normalized value of the individual calibration parameters for the TC FC electrochemical model.

calibration parameters being fitted, aforementioned AIC infromation criteria was used, which has a penalising term considering the number of calibration parameters and the amount of experimental data that is used in the calibration procedure (see Equation (52)). Thus, the AIC estimates the quality of each of the electrochemical models, relative to each other and it could provide a means for model selection.

An analysis of the results with both criteria show little to no change in the relative criterion output value, based on which it can be concluded that any of the presented criteria can be used without fear of obtaining distorted results for the set of electrochemical models at hand. It can also be concluded that the newly derived electrochemical model behaves very well when calibrated to single or multiple experiments, which hints that its prediction capability and generality are among the best in the present collection of electrochemical models.

4.3. Extrapolation and interpolation validation

Improved extrapolation capabilities combined with good prediction capability and generality of the model enable the use of much smaller experimental data sets to determine calibration parameters, while still obtaining good agreement between model and experimental data outside the trained variation space. To assess the extrapolation and interpolation capabilities of the model outside the trained variation space, four permutations of the four available polarisation curves were made, to obtain four sets of three polarisation curves, each set missing a different one. These were used for parameter calibration and the missing one was used as a validation data set. Thereby, two extrapolation sets:

- calibrated on 1., 2., 3. validated on 4.
- calibrated on 2., 3., 4. validated on 1.;

and two interpolation sets:

- calibrated on 1., 2., 4. validated on 3.;
- calibrated on 1., 3., 4. validated on 2.;

were obtained. The numbering of the polarisation curves is shown in Fig. 4.

4.3.1. Extrapolation

The electrochemical models were calibrated on the first three and validated on fourth polarisation curve. Results show (Fig. 6a), that the TC FC electrochemical model has the smallest deviations from the validation experimental data set.

When calibrating, the region of polarisation curve, where activation losses are the most prominent, should always be included in order to achieve the best results. Otherwise it is highly likely that the parameters describing activation overpotential will not be physically plausible, which can affect the rest of parameters as well. This was confirmed with the results presented in Fig. 6b, where it can be clearly seen that the extrapolated results for the bottom polarisation curve, give a very poor fit in the case of otherwise very well behaved models such as the newly derived TC FC electrochemical model and Kulikovsky's model [32].

4.3.2. Interpolation

Results obtained by interpolation are generally more in agreement with experimental data, which is to be expected due to the fact that these models have been trained on data set with all the boundary points included, therefore the calibration parameters, with which the optimization minima is obtained, ensure that all the operation points between the boundaries will not deviate much from obtained experimental data. Based on the results presented in Fig. 6c and d, Gu's [29] and the TC FC electrochemical model assure attainment of one of the best results when interpolating operational data.

4.4. Convergence speed assessment with Monte Carlo like parameter sensitivity analysis

Besides the quality of the obtained fit, it is of utmost importance that the electrochemical model enables fast convergence to the global minima of the optimization problem, especially if the model is to be used for evaluation of SOH parameters as a HiL application using only polarisation curves or data obtained from several individual operational points.

To test this aspect of the models, a genetic optimization algorithm (*'ga'* [37]) was run for single and multiple polarisation curves as described in Section 3.5. Due to the computational burden of this model analysis step, only three of the best performing models listed in Sections 4.2 and 4.3 were picked for further analysis. These are in no particular order: Gu's [29], Kulikovsky's [32] and the TC FC electrochemical model with 9 and 7 calibration parameters.

The obtained results are presented in Table 2 and values of standard deviation show that the models which are most invariant to the initial variation of parameters are Kulikovsky's model [32] and the TC electrochemical model with a reduced set of calibration parameters, which both show a similar standard deviation of RMSD. However, the TC electrochemical model has on average a much lower RMSD value. It can be also observed that the TC FC electrochemical model with a full set of calibration parameters has a higher standard deviation, thus hinting towards higher convergence times. Furthermore, the overall fitness of the polarisation curves obtained for single experiment is significantly lower in comparison to multiple experiments, which is to be expected due to the fact that the model is optimized for only one set of operational conditions.

Determination of how well and how fast models are being calibrated on the global scale does not offer any insight in how well individual parts of the polarisation curve are being calibrated. Some information about this can be roughly estimated by looking at the results of the calibrated model presented in Fig. 4. To assess this problem, the covariance of the calculated voltage for 500 sets of obtained calibration parameters was obtained with the aim of determining which parts of the polarisation curves are better defined with a set of calibration parameters. Results of this analysis are presented in Fig. 7a, b and 7c, where four polarisation curves and four curves describing covariance at each of the operational points on the polarisation curve are shown. Even though the covariance values obtained are very small, they offer a unique insight into the repeatability of determining calibration parameters and their effects on individual parts of the polarisation curve. In general, higher covariance values are obtained in regions of activation losses and concentration losses, which tells us that parameters influencing this parts of polarisation curve are harder to determine for the data set at hand. Only the first curve in the case of the TC electrochemical model behaves differently, where its values are the highest in the region of ohmic losses, however the covariance values are a magnitude lower compared to other models. Covariance values are thus lowest for the TC electrochemical model and highest for Gu's model [29], which is in direct correlation with the results presented in Table 2, where Gu's model [29] has the highest and the TC electrochemical model has the lowest standard deviation. However, this is not to be confused with the quality of the obtained fit, which was previously assessed based on the RMSD values presented in Table 2.

Table 2
Average value and standard deviation of RMSD values obtained with 500 Monte Carlo like simulations with genetic algorithm (*'ga'* [37]) for Gu's [29], Kulikovsky's [32] and TC electrochemical model with 9 and 7 calibration parameters.

	Average value		Standard deviation	
	Single exp.	Multiple exp.	Single exp.	Multiple exp.
Gu et al. [29]	0,01034	0,00785	3,59E-08	2,94E-07
Kulikovsky [32]	0,00694	0,00860	1,81E-10	1,19E-08
9 calib. param.	0,00393	0,00561	1,12E-08	2,86E-10
7 calib. param.	0,00393	0,00561	4,13E-10	5,97E-11

5. Conclusions

The newly derived quasi-1D TC FC electrochemical model exhibits high generality and prediction capability, which position the proposed modelling framework beyond currently published state-of-the-art models for virtual observers. Derivation of the BV equation and the proposed use of its mathematical equivalent with the sinus hyperbolicus term results in an easily invertible expression valid for all current density regions, while enabling a thermodynamically consistent treatment of forward and backward reaction direction for both the anode and cathode side. The consequential inherent conclusions of this investigation can be summarized as:

1. The newly derived 0D TC FC electrochemical model and its extension with a simplified 1D approach of accommodating the diffusive transport of species in the GDL exhibit direct correlation with the SoH parameters of the FC. Some of these are the intrinsic exchange current density, the activation energy on the anode and cathode side and the lumped parameters for reaction rates on both sides. Furthermore, further analysis of the combined diffusive parameters in the future would enable estimating the change of hydrophobic properties of the GDL.
2. The proposed methodology and framework for an in-depth electrochemical model assessment enables the determination of the optimal set of calibration parameters and proposes possible model reductions. Application of this approach to the newly derived quasi-1D TC FC electrochemical model results in two reduced versions of the model, namely a general version with 7 calibration parameters and an isothermal version with 5 fitting parameters. In addition, obtainment of better fit quality and the determination of calibration parameters with higher certainty, based on the data set at hand is enabled, which results in a simplified and sped up calibration procedure.
3. The newly derived quasi-1D TC FC electrochemical model shows the best results when taking into account generality and the prediction capability of the model. It adequately replicates experimental voltage vs. current profiles and confirm its very good extrapolation capabilities for operation points outside the calibrated variation space of the parameters, thus proving its robustness. Additionally, the newly developed model retains the best results for both fitting errors and computational times needed for obtaining the global minima for a set of calibration parameters on the variety of selected data sets used in this paper.

Declaration of competing interest

The authors declare that they have no known competing financial interests or personal relationships that could have appeared to influence the work reported in this paper.

Acknowledgements

The research is partially funded by the Slovenian Research Agency (research core funding No. P2-0401), by the CD Laboratory for Innovative Control and Monitoring of Automotive Powertrain Systems and by the Austrian Research Promotion Agency (research project no. 854867: SoH4PEM).

Appendix B. Supplementary data

Supplementary data to this article can be found online at https://doi.org/10.1016/j.jpowsour.2020.227930.

Appendix A. Simplifications of the BV equation in published models

Tafel equation written with abbreviations used in the presented paper:

$$j_c = \mathrm{e}^{-\frac{A_0}{k_B T}} \mathrm{e}^{-\frac{\Delta s_c^0}{k_B T}} \mathrm{e}^{-\frac{\alpha_c \Delta s_c \left(T-T^0\right)}{k_B T}} \mathrm{e}^{-\alpha_c \cdot \ln\left(\frac{k^*_{RDC}}{k_{OXC}}\right)} \left(\tilde{C}_{O_2}\right)^{(1-\alpha_c)} \cdot \left(\tilde{C}_{H_2O}\right)^{2\alpha_c} k^*_{RDC} \cdot \mathrm{e}^{-\frac{\alpha_c e_0 Z_c \eta_c}{k_B T}} \tag{A.1}$$

$$j_a = \mathrm{e}^{-\frac{B_0}{k_B T}} \mathrm{e}^{-\frac{\Delta s_a^0}{k_B T}} \mathrm{e}^{-\frac{\alpha_a \Delta s_a \left(T-T^0\right)}{k_B T}} \mathrm{e}^{-\alpha_a \cdot \ln\left(\frac{k_{OXA}}{k^*_{RDA}}\right)} \left(\tilde{C}_{H_2}\right)^{(2\alpha_a)} \cdot k^*_{RDA} \cdot \mathrm{e}^{\frac{\alpha_a e_0 Z_a \eta_a}{k_B T}} \tag{A.2}$$

Expressions in Equations (A.1) and (A.2) are easily rearranged (by taking natural logarithm) to obtain expressions for the overpotentials:

$$\eta_c = -\frac{A_0}{\alpha_c e_0 Z_c} - \frac{\Delta g_c^0}{\alpha_c e_0 Z_c} - \frac{\alpha_c \Delta s_c \left(T-T^0\right)}{\alpha_c e_0 Z_c} - \frac{k_B T}{\alpha_c e_0 Z_c} \ln\left(\frac{j_c}{\left(\tilde{C}_{O_2}\right)^{(1-\alpha_c)} \left(\tilde{C}_{H_2O}\right)^{2\alpha_c} \left(k^*_{RDC}\right)^{(1-\alpha_c)} \left(k_{OXC}\right)^{\alpha_c}}\right) \tag{A.3}$$

$$\eta_a = -\frac{B_0}{\alpha_a e_0 Z_a} - \frac{\Delta g_a^0}{\alpha_a e_0 Z_a} - \frac{\alpha_a \Delta s_a \left(T-T^0\right)}{\alpha_a e_0 Z_a} - \frac{k_B T}{\alpha_a e_0 Z_a} \ln\left(\frac{j_a}{\left(\tilde{C}_{H_2}\right)^{(2\alpha_a)} \left(k^*_{RDA}\right)^{(1+\alpha_a)} \left(k_{OXA}\right)^{-\alpha_a}}\right) \tag{A.4}$$

Correction of Tafel equation as presented in Refs. [31–33] using consistent abbreviations from the present paper:

$$\eta_c = -\frac{A_0}{\alpha_c e_0 Z_c} - \frac{\Delta g_c^0}{\alpha_c e_0 Z_c} - \frac{\alpha_c \Delta s_c \left(T-T^0\right)}{\alpha_c e_0 Z_c} - \frac{k_B T}{\alpha_c e_0 Z_c} \cdot \operatorname{arcsinh}\left(\frac{j_c}{\left(\tilde{C}_{O_2}\right)^{(1-\alpha_c)} \left(\tilde{C}_{H_2O}\right)^{2\alpha_c} \left(k^*_{RDC}\right)^{(1-\alpha_c)} \left(k_{OXC}\right)^{\alpha_c}}\right) \tag{A.5}$$

References

[1] N.K. Medora, 7 - electric and plug-in hybrid electric vehicles and smart grids, in: B. W. D'Andrade (Ed.), The Power Grid, Academic Press, 2017, pp. 197–231, https://doi.org/10.1016/B978-0-12-805321-8.00007-0.

[2] C. Thomas, Fuel cell and battery electric vehicles compared, Int. J. Hydrogen Energy 34 (15) (2009) 6005–6020, https://doi.org/10.1016/j.ijhydene.2009.06.003.

[3] S. Jain, L. Kumar, 31 - fundamentals of power electronics controlled electric propulsion, in: M.H. Rashid (Ed.), Power Electronics Handbook, fourth ed. Edition, Butterworth-Heinemann, 2018, pp. 1023–1065, https://doi.org/10.1016/B978-0-12-811407-0.00035-0, fourth ed.

[4] I. Staffell, D. Scamman, A. Velazquez Abad, P. Balcombe, P.E. Dodds, P. Ekins, N. Shah, K.R. Ward, The role of hydrogen and fuel cells in the global energy system, Energy Environ. Sci. 12 (2019) 463–491, https://doi.org/10.1039/C8EE01157E.

[5] T.-W. Lee, A.A. Tseng, K.-S. Bae, Y.H. Do, Simulation of the proton-exchange membrane (PEM) fuel cell life-cycle performance with data-driven parameter estimation, Energy & Fuels 24 (3) (2010) 1882–1888, https://doi.org/10.1021/ef901519f.

[6] Kamran Javed, Rafael Gouriveau, Noureddine Zerhouni, Daniel Hissel, Prognostics of Proton Exchange Membrane Fuel Cells stack using an ensemble of constraints based connectionist networks, J. Power Sources 324 (2016) 745–757, https://doi.org/10.1016/j.jpowsour.2016.05.092.

[7] Rui Ma, Tao Yang, Elena Breaz, Zhongliang Li, Pascal Briois, Gei Gao, Data-driven proton exchange membrane fuel cell degradation predication through deep learning method, Appl. Energy 231 (2018), https://doi.org/10.1016/j.apenergy.2018.09.111.

[8] R. Silva, R. Gouriveau, S. Jemeï, D. Hissel, L. Boulon, K. Agbossou, N. Yousfi Steiner, Proton exchange membrane fuel cell degradation prediction based on Adaptive Neuro-Fuzzy Inference Systems, Int. J. Hydrogen Energy 39 (21) (2014) 11128–11144, https://doi.org/10.1016/j.ijhydene.2014.05.005.

[9] H. Liu, J. Chen, C. Zhu, H. Su, M. Hou, Prognostics of proton exchange membrane fuel cells using A model-based method, 20th, IFAC World Congr. 50 (1) (2017) 4757–4762, https://doi.org/10.1016/j.ifacol.2017.08.947.

[10] R. Bellman, R. Corporation, K.M.R. Collection, Dynamic Programming, Rand Corporation Research Study, Princeton University Press, 1957.

[11] J. Kim, S. Lee, S. Srinivasan, C.E. Chamberlin, Modeling of proton exchange membrane fuel cell performance with an empirical equation, J. Electrochem. Soc. 142 (8) (1995) 2670–2674, https://doi.org/10.1149/1.2050072.

[12] G. Squadrito, G. Maggio, E. Passalacqua, F. Lufrano, A. Patti, An empirical equation for polymer electrolyte fuel cell (PEFC) behaviour, J. Appl. Electrochem. 29 (12) (1999) 1449–1455, https://doi.org/10.1023/A:1003890219394.

[13] D. Chu, R. Jiang, C. Walker, Analysis of PEM fuel cell stacks using an empirical current–voltage equation, J. Appl. Electrochem. 30 (3) (2000) 365–370, https://doi.org/10.1023/A:1003905109007.

[14] Z. Xia, S. Chan, Analysis of carbon-filled gas diffusion layer for H2/air polymer electrolyte fuel cells with an improved empirical voltage–current model, Fuel Cell. 32 (7) (2007) 878–885, https://doi.org/10.1016/j.ijhydene.2006.12.013.
[15] J.H. Lee, T.R. Lalk, A.J. Appleby, Modeling electrochemical performance in large scale proton exchange membrane fuel cell stacks, J. Power Sources 70 (2) (1998) 258–268, https://doi.org/10.1016/S0378-7753(97)02683-9.
[16] S.D. Fraser, V. Hacker, An empirical fuel cell polarization curve fitting equation for small current densities and no-load operation, J. Appl. Electrochem. 38 (4) (2008) 451–456, https://doi.org/10.1007/s10800-007-9458-2.
[17] C.K. Poh, Z. Tian, N. Bussayajarn, Z. Tang, F. Su, S.H. Lim, Y.P. Feng, D. Chua, J. Lin, Performance enhancement of air-breathing proton exchange membrane fuel cell through utilization of an effective self-humidifying platinum–carbon catalyst, J. Power Sources 195 (24) (2010) 8044–8051, https://doi.org/10.1016/j.jpowsour.2010.06.103.
[18] L. Pisani, G. Murgia, M. Valentini, B. D'Aguanno, A new semi-empirical approach to performance curves of polymer electrolyte fuel cells, J. Power Sources 108 (1) (2002) 192–203, https://doi.org/10.1016/S0378-7753(02)00014-9.
[19] S. Haji, Analytical modeling of PEM fuel cell i–V curve, Renew. Energy 36 (2) (2011) 451–458, https://doi.org/10.1016/j.renene.2010.07.007.
[20] D. Hao, J. Shen, Y. Hou, Y. Zhou, H. Wang, An improved empirical fuel cell polarization curve model based on review analysis, Int. J. Chem. Eng. 2016 (2016) 10.
[21] M.E. Youssef, K. AL-NAdi, M. Khalil, Lumped model for proton exchange membrane, Fuel Cell 5 (2010).
[22] J. Larminie, Fuel cell systems explained/James Larminie, Andrew dicks, no, J. Wiley, Chichester, West Sussex, 2003. Accessed from, https://nla.gov.au/nla.cat-vn838113.
[23] J.C. Amphlett, R.M. Baumert, R.F. Mann, B.A. Peppley, P.R. Roberge, T.J. Harris, Performance modeling of the ballard mark IV solid polymer electrolyte fuel cell: II . Empirical model development, J. Electrochem. Soc. 142 (1) (1995) 9–15, https://doi.org/10.1149/1.2043959.
[24] R.F. Mann, J.C. Amphlett, M.A. Hooper, H.M. Jensen, B.A. Peppley, P.R. Roberge, Development and application of a generalised steady-state electrochemical model for a PEM fuel cell, J. Power Sources 86 (1) (2000) 173–180, https://doi.org/10.1016/S0378-7753(99)00484-X.
[25] J.M. Correa, F.A. Farret, L.N. Canha, M.G. Simoes, An electrochemical-based fuel-cell model suitable for electrical engineering automation approach, IEEE Trans. Ind. Electron. 51 (5) (2004) 1103–1112, https://doi.org/10.1109/TIE.2004.834972.
[26] C. Robin, M. Gerard, A.A. Franco, P. Schott, Multi-scale coupling between two dynamical models for PEMFC aging prediction, Int. J. Hydrogen Energy 38 (11) (2013) 4675–4688, https://doi.org/10.1016/j.ijhydene.2013.01.040.
[27] M. Chandesris, R. Vincent, L. Guetaz, J.-S. Roch, D. Thoby, M. Quinaud, Membrane degradation in PEM fuel cells: from experimental results to semi-empirical degradation laws, Int. J. Hydrogen Energy 42 (12) (2017) 8139–8149, https://doi.org/10.1016/j.ijhydene.2017.02.116.
[28] H. Weydahl, M.S. Thomassen, B.T. Børresen, S. Møller-Holst, Response of a proton exchange membrane fuel cell to a sinusoidal current load, J. Appl. Electrochem. 40 (4) (2010) 809–819, https://doi.org/10.1007/s10800-009-0064-3.
[29] W. Gu, D.R. Baker, Y. Liu, H.A. Gasteiger, Proton exchange membrane fuel cell (PEMFC) down-the-channel performance model, in: Handbook of Fuel Cells, American Cancer Society, 2010, https://doi.org/10.1002/9780470974001.f500044.
[30] S. Chan, K. Khor, Z. Xia, Complete polarization model of a solid oxide fuel cell and its sensitivity to the change of cell component thickness, J. Power Sources 93 (2001) 130–140, https://doi.org/10.1016/S0378-7753(00)00556-5.
[31] B. Laoun, Simulation of PEMFC performance 14, 2011, pp. 441–448.
[32] A.A. Kulikovsky, A physically–based analytical polarization curve of a PEM fuel cell, J. Electrochem. Soc. 161 (3) (2014) F263–F270, https://doi.org/10.1149/2.028403jes.
[33] A. Kulikovsky, Anal. Model. Fuel Cell. (2010), https://doi.org/10.1016/C2009-0-30566-8.
[34] R. O'Hayre, S. Cha, W. Colella, F. Prinz, Fuel Cell Fundamentals, Wiley, 2009.
[35] M. Mench, Fuel Cell Engines, Wiley, 2008.
[37] MATLAB, Optimization Toolbox Release, The MathWorks, Inc., Natick, Massachusetts, United States, 2018.
[38] P. Pei, X. Yuan, J. Gou, P. Li, Dynamic response during pem fuel cell loading-up, Materials 2 (3) (2009) 734–748, https://doi.org/10.3390/ma2030734.
[39] A. Arce, A.J. del Real, C. Bordons, D.R. Ramirez, Real-time implementation of a constrained mpc for efficient airflow control in a pem fuel cell, IEEE Trans. Ind. Electron. 57 (6) (2010) 1892–1905, https://doi.org/10.1109/TIE.2009.2029524.
[40] J. Luna, S. Jemei, N. Yousfi-Steiner, A. Husar, M. Serra, D. Hissel, Nonlinear predictive control for durability enhancement and efficiency improvement in a fuel cell power system, J. Power Sources 328 (2016) 250–261, https://doi.org/10.1016/j.jpowsour.2016.08.019.